Global and Planetary Change 216 (2022) 103904

Contents lists available at ScienceDirect

Global and Planetary Change

journal homepage: www.elsevier.com/locate/gloplacha

Organic geochemistry evidence for wildfire and elevated pO_2 at the Frasnian–Famennian boundary

Zeyang Liu [a], Hui Tian [a,*], David Selby [b], Jianfang Hu [a], D. Jeffrey Over [c]

[a] State Key Laboratory of Organic Geochemistry, CAS Center for Excellence in Deep Earth Science, Guangzhou Institute of Geochemistry, Chinese Academy of Sciences, Guangzhou 510640, China
[b] Department of Earth Sciences, University of Durham, Durham DH1 3LE, UK
[c] Department of Geological Sciences, SUNY College at Geneseo, Geneseo, NY 14454, USA

ARTICLE INFO

Keywords:
Atmospheric oxygen level
Polycyclic aromatic hydrocarbons
F–F
Terrestrial input
pCO_2 drawdown
Weathering

ABSTRACT

The Devonian experienced radiations of plants and animals, as well as a major mass extinction event during the Frasnian–Famennian (F—F) interval. Proposed triggers have been linked to volcanism, extraterrestrial impact, sea-level fluctuations, and climate cooling, etc. However, the nature of the wildfires and its role in the biotic evolution have been rarely investigated for the F—F interval. Here, we report organic geochemistry proxies (e.g., polycyclic aromatic hydrocarbons, PAHs) in three sections from New York (USA) to further investigate the wildfire activity and its potential link with the environmental and biotic perturbations around the F—F interval. The studied intervals are dominated by three-ring PAHs which display an increasing abundance stratigraphically towards the F—F boundary (FFB). An increase of 6-ring over 3-ring PAHs across the FFB is also observed for the studied sections, indicating elevated burning temperature. Additionally, slightly increased plant wax abundance and average chain length values and relatively constant Pr/Ph ratios are observed. Collectively, these results propose an increased burning frequency over the F—F interval caused by elevated pO_2 level, rather than a change in aridity. Terrestrial input only slightly increased across the FFB, and there is limited evidence for ocean anoxia. This correlates with the hypothesis that pCO_2 drawdown and climate cooling could have been a driving mechanism of the F—F biocrisis.

1. Introduction

The Earth witnessed dramatic changes during the Devonian. Within these changes, the evolution and widespread rapid terrestrial invasion of plants increased the atmospheric levels of oxygen (pO_2; Glasspool and Scott, 2010). The expansion of terrestrial plants provided the habitat and oxygen necessary for the terrestrial evolution of life on land and ultimately led to the appearance of larger body size animals that had a higher oxygen demand (Dahl et al., 2010). In addition to the radiation of life over this period, the Late Devonian also records one of the "big five" mass extinction events – the Frasnian–Famennian (F—F) biocrisis (Stanley, 2016). Possible causes of this catastrophic event have been attributed to, but not limited to, volcanism (Racki et al., 2018), extraterrestrial impact (Claeys et al., 1992, although this has since been refuted by multiple studies, e.g. Percival et al., 2018), ocean anoxia and/or euxinia (e.g., Bond et al., 2004; Bond and Wignall, 2008; Carmichael et al., 2014), sea-level fluctuation (Copper, 2002; Johnson et al., 1985), climate cooling (Joachimski et al., 2009; Huang et al., 2018), and orbital forcing (Lu et al., 2021).

Wildfires played an important role in regulating the Earth's environment (Glasspool et al., 2015). In the geological record, fire frequency is closely linked with pO_2 and has been extensively studied for intervals with major climatic and biotic perturbations, such as the Permian–Triassic mass extinction (Shen et al., 2011). In contrast, a wildfire event has been rarely studied for the F—F interval. Previously, the F—F interval has been taken to represent an interval during which wildfire events are sparse (Scott and Glasspool, 2006; Rimmer et al., 2015). No fossil charcoal has been found in this interval, despite the availability of terrestrial plants to be burnt (Stein et al., 2012). This leads to the conclusion of a low pO_2 level during the F—F interval such that wildfire activity cannot be sustained (Rimmer et al., 2015). Yet, more recently, fossil charcoal (inertinite) has been reported from five F—F sections in the western New York State (USA), thus providing support for a history of wildfires during the F—F interval (Liu et al., 2020).

* Corresponding author.
E-mail address: tianhui@gig.ac.cn (H. Tian).

https://doi.org/10.1016/j.gloplacha.2022.103904
Received 11 December 2021; Received in revised form 16 July 2022; Accepted 28 July 2022
Available online 31 July 2022

Despite the observation of inertinite in the New York State F—F sections, the trends in the inertinite abundance profiles are not uniform, which hampered the interpretation of the role of wildfires in the F—F mass extinction, and highlights the need for more comprehensive studies of wildfire events over the F—F interval. Here, we report PAHs data, coupled with Pr/Ph, plant wax abundance and average chain length data from three New York sections to further constrain the timing of wildfire events. The concentrations of PAHs, unlike inertinites, do exhibit trends in changes of fire intensity across the F—F boundary. As such, we discuss the potential link between wildfire events and the biotic and climatic perturbations during the Late Devonian.

2. Samples

In this study, three outcrop sections (Beaver Meadow Creek, BMC; Irish Gulf, IG; Walnut Creek Bank, WCB) from western New York state were investigated (Fig. 1). These records represent slope to basin deposits within the northern Appalachian foreland basin, and are interpreted to be proximal to distal deposits in terms of paleoceanography (see inserted map of Fig. 1) (Sageman et al., 2003). In all three sections, the studied interval is composed of the latest Frasnian–earliest Famennian Hanover Formation and the early Famennian Dunkirk Formation. The Hanover Formation is composed of light gray, silty shales (less than 1 wt% total organic carbon, TOC) interbedded with black silty shales that are rich in organic matter (~ 1–6 wt% TOC) and thermally mature (BR_o ~ 0.6%, solid bitumen reflectance; Liu et al., 2020). Evidence of bioturbation is observed for the gray shale, and hosts poorly preserved brachiopods and bivalves (Over, 1997, 2002; Boyer et al., 2021). The black shales are finely laminated and rich in pyrite, an indication of deposition in an anoxic/dysoxic environment (Boyer et al., 2021; Lash, 2017; Sageman et al., 2003). Overlying the Hanover Formation, the Dunkirk Formation contains thick beds of black shale (Over, 1997). In the stratigraphic records studied here, the F—F boundary is defined by the first occurrence of the conodont *Palmatolepis triangularis* (Fig. 2; Klapper et al., 1993; Over, 1997, 2002; see also Spalletta et al., 2017) and occurs as a regionally continuous bed of black shale that is taken to be equivalent to the Upper Kellwasser Horizon (Kelly et al., 2019; Cohen et al., 2021; Uveges et al., 2019).

3. Methods

Across the F—F boundary interval, black shales were sampled at a 2–5 cm stratigraphic resolution. Above and below the F—F boundary, the black shale units were sampled at a lower resolution of approximately 5–10 cm. Samples were powdered (~200 mesh) using a Zirconium dish and puck mill using a shatterbox.

3.1. Total organic carbon and organic carbon isotope

Total organic carbon (TOC) content and organic carbon isotope ($\delta^{13}C_{org}$) determinations were analyzed at the State Key Laboratory of Organic Geochemistry at Guangzhou Institute of Geochemistry. Samples were acidified: ~1 g of powder was mixed with 15 mL 2 N HCl and left for 24 h. Acid was decanted and then the samples were rinsed three times with DI water to neutralize the acid. Samples were then dried in an oven at 60 °C for 2–3 days until their weights are constant. The TOC measurements were conducted using a Leco CS230 carbon/sulfur analyser. The samples were further ground to fine powder using an agate pestle and mortar and loaded into tin capsules for carbon isotope measurement. Carbon isotope values ($\delta^{13}C_{org}$) were analyzed using a Thermo Delta XL Plus isotope ratio mass spectrometer. Data are reported in delta notation (δ) in per mil (‰) relative to the Vienna Peedee Belemnite (VPDB). The analytical uncertainty on internal standards throughout the analytical run was ±0.09 ‰ (2σ, $n = 10$).

3.2. Molecular organic geochemistry

Polycyclic aromatic hydrocarbons (PAHs) and saturated hydrocarbons analyses were conducted in the State Key Laboratory of Organic Geochemistry at Guangzhou Institute of Geochemistry. Before analyses, all the glassware, aluminum foil, silica gel, quartz sand and quartz wool were baked in an oven at 500 °C for 6 h to remove potential organic contaminants. Sample powders (~10 g) were extracted with mixture solvents of dichloromethane/methanol (9:1, *v*/v) in a Soxhlet extractor

Fig. 1. Paleogeography map showing location of the Appalachian Basin (open square) in North America (after Liu et al., 2020). Inserted map shows the present-day New York State sample locations – a: Walnut Creek Bank, b: Irish Gulf, c: Beaver Meadow Creek). The orange circle represents the Belgium Frasnian–Famennian sections where a wildfire event at the F—F boundary is also inferred (Kaiho et al., 2013).

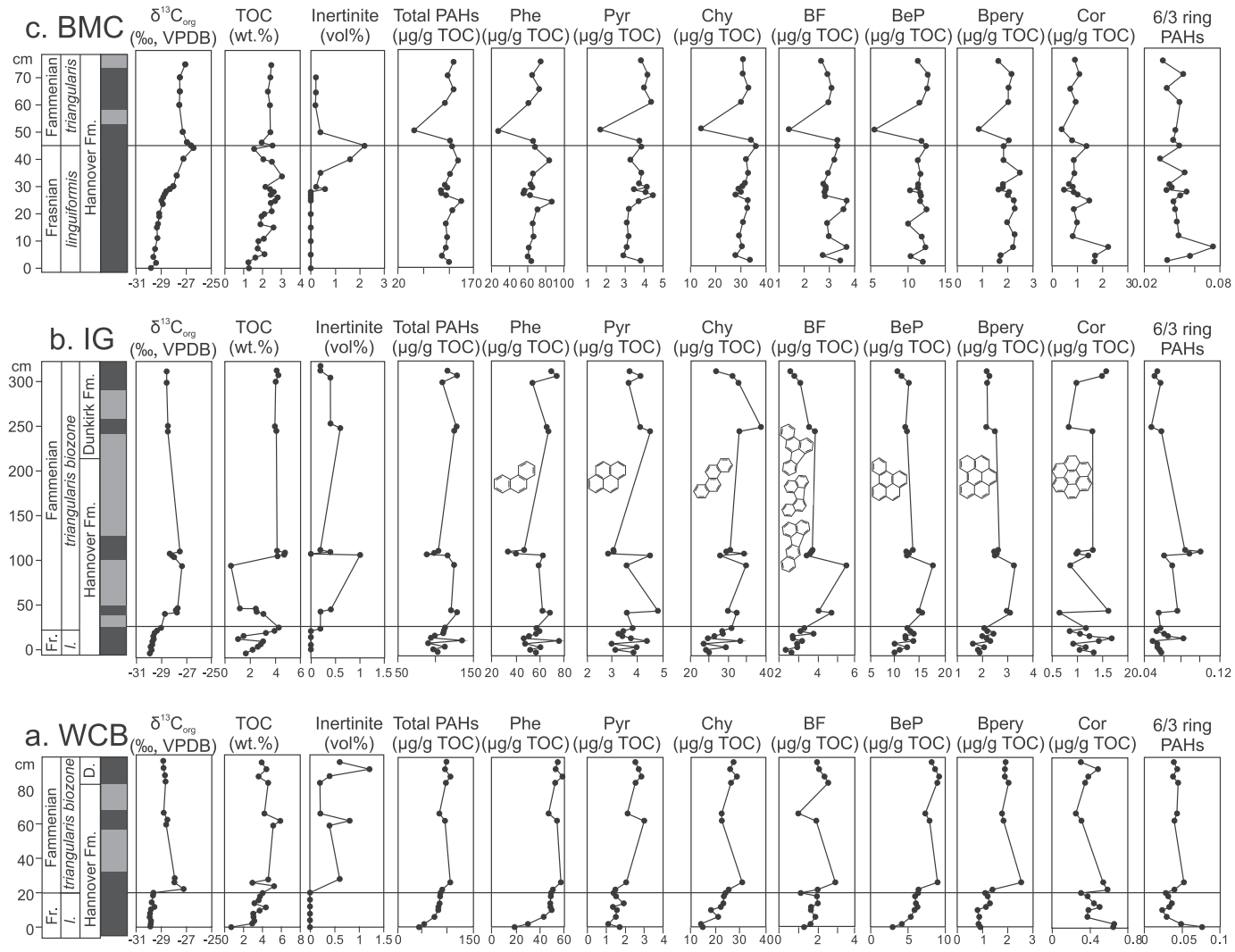

Fig. 2. $\delta^{13}C_{org}$ stratigraphy and biomarkers from three F—F sections, New York State, USA. Abbreviations: Phe, phenanthrene; Pyr, pyrene; Chy, chrysene; BF, benzofluoranthenes; BeP, benzo[*e*]pyrene; BPery, benzo[*ghi*]perylene; Cor, coronene; PWRA, plant wax relative abundance; ACL, average chain length. Inertinite abundance data are from Liu et al. (2020). a: Walnut Creek Bank (WCB); b: Irish Gulf (IG); c: Beaver Meadow Creek (BMC).

for 72 h. The extracts were then separated into saturated, aromatic, and polar fraction using silica gel column chromatography (~15 cm height). The volume of the silica gel column was determined by counting the liquid volume of *n*-hexane from the first aliquot loaded to the first volume eluted (dead volume, 1dv). Then the saturated fraction was eluted using three times column volume of *n*-hexane (3dv). The aromatic fraction was eluted with a 3dv dichloromethane/*n*-hexane (1:1, v/v) solution. The polar fraction was eluted with methanol (Song et al., 2020). The eluent fractions were then concentrated to a final volume of 0.3 mL.

The PAHs were analyzed using a Shimadzu gas chromatography–mass spectrometry (GC/MS-QP2010) with an electron impact ion source at 70 eV. The chromatograph was equipped with a HP-5MS column (30 m × 0.25 mm, film thickness 0.25 μm). Approximately 1 μL of each aromatic fraction was injected in splitless mode and operated under electron ion source (−70 eV) in full scan mode (50–550 amu). High purity helium was used as the carrier gas at a flow rate of 1 mL/min. The temperature of transfer line, injector interface and ion source were set at 290 °C, 290 °C and 250 °C, respectively. The initial oven temperature was set at 70 °C for 3 min, then raised to 290 °C at a rate of 3 °C/min, followed by a 30 min hold. The identification of compounds was based on the retention time with reference compounds and comparison of published data. Quantification of the PAHs were achieved by comparing the measured peak areas to those with known amounts of internal reference compounds (deuterated PAHs, including naphthalene-d8, acenaphethene-d10, phenanthrene-d10, chrysene-d12 and perylene-d12) that were added to the samples before extraction. The blank control recorded only the reference material which recorded no significant contamination.

The same GC–MS instrument was used for the saturated fraction. Approximately 1 μL of each extract was injected in splitless mode and operated under electron ion source (−70 eV) in full scan mode (50–550 amu). High purity helium was used as the carrier gas at a flow rate of 1 mL/min. The temperature of transfer line, injector interface and ion source were set at 290 °C, 290 °C and 250 °C, respectively. The initial oven temperature was set at 70 °C for 3 min, then raised to 300 °C at a rate of 4 °C/ min, followed by a 20 min hold. The *n*-alkanes, pristane and phytane were quantified against the internal standard *n*-C_{36}.

4. Results

4.1. Organic carbon isotope stratigraphy

A large positive carbon isotope excursion was detected in all three sections around the F—F boundary. At the BMC section, the $\delta^{13}C_{org}$ values increase from ~ −29.5 ‰ at the bottom of the section to a

maximum value of −26.4 ‰ at the F—F boundary, and then decline to ~−27.1 ‰ stratigraphically upwards. At the Irish Gulf section, $\delta^{13}C_{org}$ values gradually increase from −29.9 ‰ across the F—F boundary and reach a nadir of −27.3 ‰ about 70 cm above the F—F boundary, and then the $\delta^{13}C_{org}$ values gradually drop to ~−28.5 ‰ upwards. At the WCB section, $\delta^{13}C_{org}$ values average ~−29.7 ‰ below the F—F boundary and rise dramatically to −27 ‰ across the F—F boundary, and then slowly drop to ~−28.8 ‰ in the upper part of the section (Fig. 2).

4.2. Polycyclic aromatic hydrocarbons

In this study, phenanthrene (Phe), pyrene (Pyr), chrysene (Chy), benzofluoranthenes (BF), benzo[*e*]pyrene (BeP), benzo[*ghi*]perylene (BPery) and coronene (Cor) were chosen as wildfire proxies to track the biomass burning activity during the F—F interval (Fig. 2, Table S1). Phenanthrene and chrysene are the dominant PAHs at all three sections (generally over 75% of the total PAHs abundance). Both the five and six ring PAHs (benzofluoranthenes, benzo[*e*]pyrene, benzo[*ghi*]perylene, and coronene) have similar trends with the three and four ring PAHs (phenanthrene, pyrene, chrysene).

PAHs concentrations were normalized to the TOC for the assessment of contributions to sedimentary organic matter from forest fires (e.g., Killops and Massoud, 1992; Jiang et al., 1998; Marynowski and Simoneit, 2009; Boudinot and Sepúlveda, 2020). The detailed trends for the total PAHs concentrations were described below, and the trends with individual PAHs are plotted in Fig. 2 (Table S1). At the Beaver Meadow Creek section, the total PAHs amounts increase from ~115 μg/g TOC to 143 μg/g TOC and then drop slightly to ~105 μg/g TOC, which then further increase to 135 μg/g TOC at ~15 cm below the F—F boundary. The total PAHs values then gradually drop across the F—F boundary to 51.2 μg/g TOC, and slowly increase to ~125 μg/g TOC in the upper part of the section. At the Irish Gulf section, the total PAHs concentrations incease from ~102 μg/g TOC to 134 μg/g TOC, and then decline to 95 μg/g TOC, which then gradually increase to ~128 μg/g across the F—F boundary. The values then gradually drop to ~87 μg/g TOC, which then increase to higher values of ~121 μg/g TOC and remained at high levels upward. At the Walnut Creek Bank section, the total PAHs values increase from a low concentration of 42.6 μg/g TOC to 106.8 μg/g TOC immediately above the F—F boundary, which then drop to 83.6 μg/g TOC and further increase to 105.4 μg/g TOC. The total PAHs values then drop to slightly lower values upsection.

At the Beaver Meadow Creek section, the 6/3-ring ratios increase from 0.038 to 0.074 at the base of the section, which then decrease to 0.047 and remain relatively constant at ~0.045 upward through the F—F boundary interval. At the Irish Gulf section, the 6/3-ring ratios express a peak from 0.057 to 0.083 about 10 cm below the F—F boundary. The 6/3-ring values then increase to 0.102 above the F—F boundary, which then decrease to ~0.05 in the upper part of the section. At the Walnut Creek Bank section, the 6/3-ring ratios decline from 0.08 to 0.024 below the F—F boundary, which then increase to 0.053 immediately above the F—F boundary. The 6/3-ring ratios values then decrease to ~0.04 upsection (Fig. 2).

5. Discussion

5.1. Evaluation of thermal maturity and weathering effect on PAHs

In nature, PAHs are generated by incomplete combustion of organic materials (Lima et al., 2005). It has been used as a well-established wildfire proxy and applied in several climatic and biotic perturbation intervals in the Earth history (Finkelstein et al., 2005; Kaiho et al., 2021; Kaiho et al., 2013; Marynowski and Filipiak, 2007). However, prior to interpreting of PAH data as a primary proxy for wildfire events, potential alteration from secondary processes such as weathering and/or thermal maturity need to be carefully evaluated (Marynowski et al., 2011). Previous thermal maturity proxies of solid bitumen reflectance (BR_o, ~0.7%) and T_{max} values (~445 °C) suggest a low thermal maturity of the samples throughout these F—F sections (Liu et al., 2020). Furthermore, there is no correlation between PAHs concentrations and thermal maturity proxies from saturates (e.g., Ts/[Ts + Tm] and 22S/[22S + 22R]C_{31}homohopane; Fig. 3), and highly pericondensed compounds like benzofluoranthenes, benzo[*e*]pyrene, benzo[*ghi*]perylene and coronene are minimally susceptible to thermal alteration and biodegradation (Jiang et al., 1998; Schmidt and Noack, 2000). Further, early studies have demonstrated that pyrene, benzo[*ghi*]perylene, and coronene are dominant types of PAHs derived from forest fires (Venkatesan and Dahl, 1989; Killops and Massoud, 1992; Masclet et al., 1995; Arinobu et al., 1999), and their condensed structures make them resistant to degradation (Killops and Massoud, 1992). Weathering processes have been demonstrated to be able to alter the PAHs record (Marynowski et al., 2011). However, in this study, fresh outcrop samples were collected and extra care has been taken to remove the potential weathered surface. Furthermore, other geochemistry analyses such as osmium isotope ($^{187}Os/^{188}Os$, or Os_i), which is extremely sensitive to weathering, have yielded geologically meaningful Os_i values that are identical to Os_i values from core records (see Fig. 7 in Liu et al., 2020) and are equivalent to Os_i values from other sections (Gordon et al., 2009; Harris et al., 2013; Jaffe et al., 2002; Turgeon et al., 2007). Therefore, we consider the trends of PAHs compounds in the F—F strata to reflect a primary depositional signature and might suggest enhanced frequency of wildfire activity towards the F—F (Fig. 2). The appearance of inertinite from these sections further demonstrate that the PAHs are of fire origin, although the inertinite and PAHs profiles do not correlate (Fig. 2; Liu et al., 2020). The maximum concentrations of PAHs occur before the maximal inertinite content (Fig. 2). This may be in a direct response to sea-level fall at the F—F boundary. Thus, possibly more inertinite was transported to the sea due to the shorter transport distance. In contrast, PAHs were transported via aerosols.

5.2. Wildfires across the F—F Interval

Although all PAHs are shown to have a combustion source (Lima et al., 2005), the distribution of PAHs in the surrounding sediments are linked to the specific burning conditions, e.g., the burning of plant community material combined with the combustion temperature (Lima et al., 2005). Moreover, the distribution of PAHs in the sedimentary record could be affected by the distance of transportation and the form (particulate/gas) of the transportation (Masclet et al., 1988, 1995). For example, benzo[*e*]pyrene and coronene are enriched in the particulate phase, whereas pyrene and fluorene are dominant in the gas phase (Masclet et al., 1988, 1995). The precipitation of PAHs during the transportation might also affect the final PAHs deposition/composition in the sedimentary record (Masclet et al., 1988, 1995). Previous investigations have suggested that the forest fire type during the F—F interval was a surface fire with burning temperature estimated between 400 and 500 °C, rather than an intensive crown fire, based on inertinite reflectance value of 1.74–3.16%. The burning material is inferred to be herbaceous and shrubby material (Liu et al., 2020). The heterogenous trends for each individual type of PAHs, and the different PAHs trends for each of the investigated sections may be linked to the special heterogeneity of wildfires and their burning temperatures, as well as the sections' distance from the land that the PAHs in the gas phase may migrate further than those in the particulate phase (Fig. 2).

At the Walnut Creek Bank section, the PAHs generally show an increase in concentration towards the F—F boundary, and the coronene concentration firstly decreases below the F—F and then increases across the F—F boundary (Fig. 2). At the Irish Gulf section, most of the PAHs show an increasing trend towards the F—F boundary, with phenanthrene, chrysene and coronene expressing a small peak below the F—F boundary (Fig. 2). The increase in the concentrations of pyrene, benzo[*ghi*]perylene, and coronene towards the F—F boundary at the Irish Gulf and Walnut Creek Bank sections might suggest increased wildfire

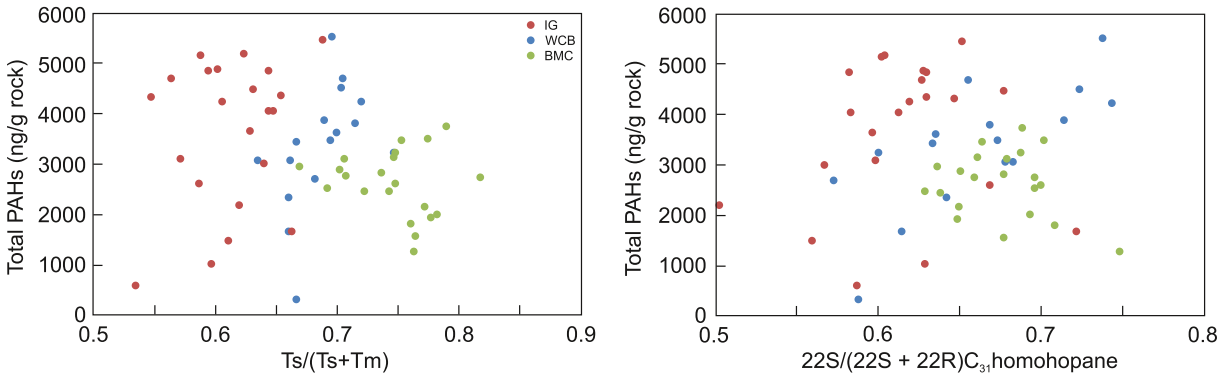

Fig. 3. Cross plots for total PAHs concentrations and thermal maturity parameters. WCB: Walnut Creek Bank (blue), IG: Irish Gulf (red), BMC: Beaver Meadow Creek (green). (For interpretation of the references to colour in this figure legend, the reader is referred to the web version of this article.)

burning frequency during the F—F interval, although the Beaver Meadow Creek section show a relatively constant profile of the PAHs concentrations (Fig. 2). High burning temperature may generate more 6-ring PAHs compared with three-ring PAHs, which could also be generated from weathering and burning of sedimentary hydrocarbons (e.g., coal; Belcher et al., 2009; Killops and Massoud, 1992, Finkelstein et al., 2005; Belcher et al., 2009). Thus, the 6/3-ring ratio has been proven to be a useful proxy to reconstruct high temperature biomass burning that occurs during forest fires, and reduce the influence of changes related weathering and burning of sedimentary hydrocarbons (Boudinot and Sepúlveda, 2020). The 6/3-ring ratio increase towards the F—F boundary at the WCB and IG sections. Moreover, an increase in the 6/3-ring ratio at the BMC section were also found, although it is slightly stratigraphically lower than that of the IG and WCB sections. The latter support an increase in frequency of wildfires and an increase in high temperature burning during the F—F interval. An increase in PAHs abundance (Cor, BPery and BeP) has also been reported for two Belgium sections and are interpreted to reflect enhanced wildfire events (Kaiho et al., 2013). The increase of resistant PAHs degradation (pyrene, benzo [*ghi*]perylene, and coronene) and the 6/3-ring ratio over the F—F interval further support the occurrence of wildfires and increased frequency towards the F—F Boundary. Nonetheless, the exact scale (global, regional, or local) of wildfires during the F—F interval remains unclear without further investigation of multiple F—F sections.

The ignition of wildfires could be caused by heat from natural lightning, volcanic activity, meteorite impact and even sparks generated by rock fall, with lightning strikes considered to be the most common ignition method (Glasspool and Scott, 2010). In the case of the wildfires around the F—F interval, volcanism could have been an alternative source of ignition. Increased mercury concentrations (which has been used as evidence for volcanic activities by several researchers) have been reported from several F—F sections (Racki et al., 2018; Kaiho et al., 2021; Liu et al., 2021; Zhao et al., 2022). Moreover, a bentonite layer has also been reported below the F—F interval, which might indicate volcanism before the F—F Boundary (Kaufmann et al., 2004). It is worth to note that the dating of the F—F boundary does not directly correlate with any major large ingeous provinces ages, and Hg enrichments might be driven by increased amounts of sulfides, organic matter and clay minerals rather than volcanism (e.g., Percival et al., 2018; Shen et al., 2020). An increase in coronene abundance for three carbonate-dominated F—F sections (Yangdi, China; Sinsin, Belgium; Coumiac, France; with TOC generally less than 0.3%) is interpreted to be the product of high-temperature country rock heating caused by the sill emplacement and/or large wildfires ignited by lava flows, rather than normal wildfires (Kaiho et al., 2021). However, in the sections from this study, no Hg (Hg/TOC) spike is detected (Liu et al., 2021), and thus the PAHs are likely produced by combustion from natural wildfires.

5.3. Implications for elevated atmospheric oxygen level

For terrestrial plant material to burn, a minimum pO_2 concentration of 16% is needed (Belcher et al., 2010). Below this level, regardless of the dryness of the organic matter, wildfire activity cannot be sustained. In general, the higher the oxygen level, the less effect the moisture content has on the ability for organic material to combust (Watson and Lovelock, 2013). In the Late Devonian, readily available combustible terrestrial organic matter comprised a developed plant community and even the appearance of small forests (Stein et al., 2012). However, the F—F interval has been considered to be an interval with few wildfire events due to suppression by low pO_2 level (~17%, Scott and Glasspool, 2006). The recovery of inertinite coupled with PAHs data in this study, further suggests the occurrence of wildfires during the F—F interval (Fig. 2). The increased PAHs concentration towards the FFB is consistant with an increase in pO_2 level over this interval as suggested by different models (Krause et al., 2018; Lenton et al., 2018; Schachat et al., 2018).

In addition to an increased pO_2 level, changes in aridity can make areas or intervals more prone to wildfire events (Heimhofer et al., 2018). Plants tend to biosynthysize longer plant cuticle wax chains to retain moisture within the leaf as a response to drier climate (Eglinton and Hamilton, 1967). The average chain length (ACL) of plant wax *n*-alkanes, as calculated by Eq. (1), has been shown to be an effective proxy for aridity (Carr et al., 2014).

$$ACL = ([nC_{27}]*27) + ([nC_{29}]*29) + ([nC_{31}]*31) + ([nC_{33}]*33) + ([nC_{35}]*35) / [nC_{27}] + [nC_{29}] + [nC_{31}] + [nC_{33}] + [nC_{35}] \quad (1)$$

However, it is noteworthy that cases have also been reported where ACL decreases in response to incresased aridity (Hoffmann et al., 2013). In addition, plant community changes can also affect the changes in ACL (Bush and McInerney, 2013; Diefendorf et al., 2011; Vogts et al., 2012). These factors all together make the interpretation of ACL data complicated.

Regardless of cause, the average chain length (ACL) in all three sections remained around 29, with the Beaver Meadow Creek (BMC) and Irish Gulf (IG) sections increasing slightly to ~29.5 below the FFB (Fig. 4). This short stratigraphic interval would be too brief for any plant community change. Rather, a transient change in aridity might be a more reasonable interpretation for these minor inceases in ACL. However, aridity change cannot account for the trend in increasing PAHs abundance in this study (Fig. 4). Thus, the increased PAHs abundance towards the FFB and above reflects enhanced wildfire frequency caused by elevated pO_2 level, potentially aided by a transient increase in aridity.

In addition to being regulated by pO_2 levels, wildfires have been proposed to have a positive feedback on the pO_2 level. As pO_2 level increases, wildfire intensity would increase and thus more charcoal would be produced and buried. This enhanced carbon burial would then further contribute to the rise of pO_2 levels (Rimmer et al., 2015). Previously, the pO_2 level has been estimated to be 24–27% (Liu et al., 2020).

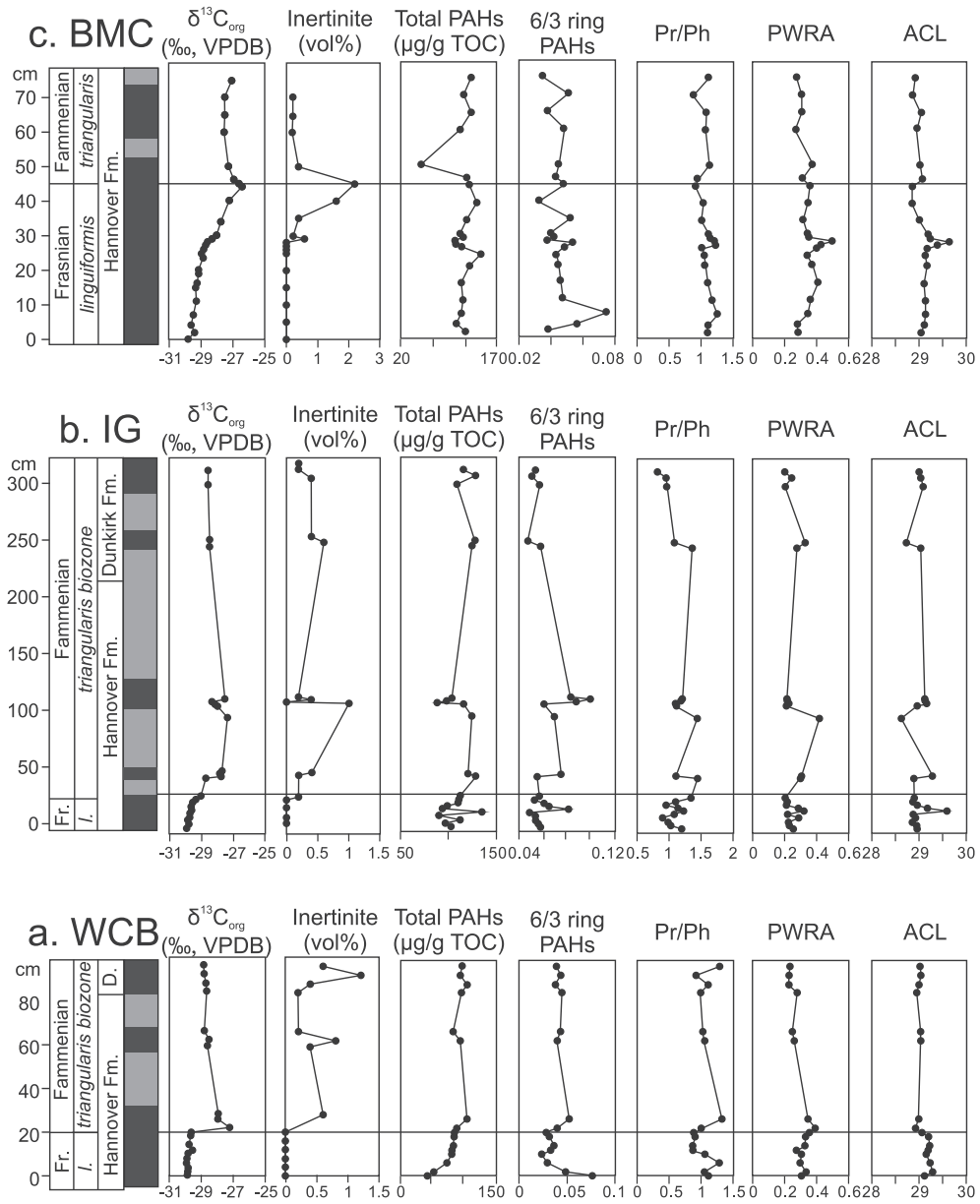

Fig. 4. Biomarkers of plant wax relative abundance (PWRA), average chain length (ACL), and pristane/phytane ratio (Pr/Ph) from three F—F sections, New York State, USA. a: Walnut Creek Bank (WCB); b: Irish Gulf (IG); c: Beaver Meadow Creek (BMC). Inertinite abundance data are from Liu et al. (2020). See text for discussion.

In addition to a sharp rise in pO_2, the ocean also experienced an episode of oxygenation across the Devonian, as evidenced by near-present day level δ^{98}Mo values for euxinic samples (2.0 ‰ compared with the modern seawater value of 2.3 ‰; Dahl et al., 2010 and reference therein). This indicates a sychronised rise in the atmospheric and oceanic oxygen contents over the Devonian (Fig. 5) although experiencing a episode of anoxia across the F—F interval (see below discussion).

5.4. Implications for the Frasnian–Famenian mass extinction

Wildfires have been proposed to destroy plant root systems and lead to enhanced continental weathering, generate soot and aerosol, and affect the carbon cycle and climate, which then are ultimately linked with major ocean anoxia or mass extinction events (e.g., Archibald et al., 2018). Inceased runoff and transport of terrestrial organic matter, including terrestrial-derived nutrients (e.g., P and N) flux to the ocean have been observed in response to modern and ancient wildfire events (Barkley et al., 2019). A slightly enhanced terrestrial input was inferred from the relative abundance of plant wax (calculated by n-$C_{27,29,31,33,35}$/n-$C_{17,19,21,27,29,31,33,35}$; Boudinot and Sepúlveda, 2020) showing a minor increase below the FFB that correlates to the ACL increase in the more proximal sections of BMC and IG. The pristane/phytane (Pr/Ph) ratio has been used as a redox indicator (lower Pr/Ph ratios indicating reducing conditions and higher ratios indicating more oxic conditions), as reducing conditions favor the conversiton of the phytyl side chain of chlorophyll to phytane whereas oxic environments encourage the conversion of phytyl to pristane (Peters et al., 2005). However, the utility of this biomarker is limited by multiple factors (Koopmans et al., 1999; Peters et al., 2005). For example, the Pr/Ph ratio may also be affected by the source of organic matter, with an increased flux of terrestrial organic matter resulting in an increase in the Pr/Ph value (Song et al., 2020). In the investigated sections, the samples are dominated by marine organic matter, with very limited terrestrial organic matter contribution (less

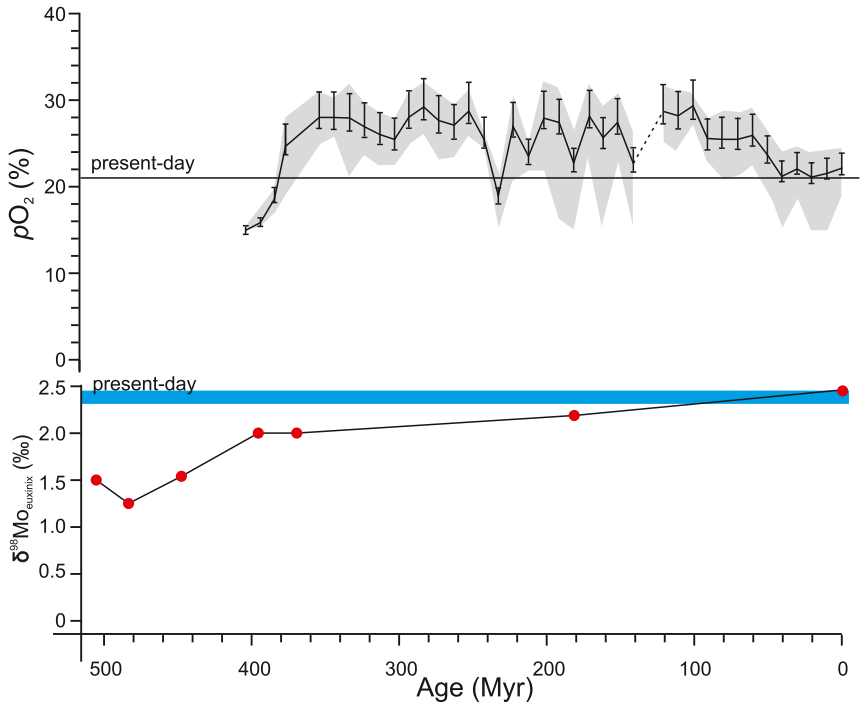

Fig. 5. Evolution curve for atmpheric oxygen level (Liu et al., 2020) and Mo isotope values of euxinic samples (Dahl et al., 2010). See text for discussion.

than 2.2%, Liu et al., 2020). Thus, we carefuly infer our Pr/Ph values here to reflect redox conditions. In the studied sections, the Pr/Ph data generally remain constant around 1 throughout the F—F interval. Further, isorenieratane and aryl isoprenoids produced by green sulfur bacteria are considered to be robust proxies for photic zone euxinia (Summons and Powell, 1986). The presence of very low absolute amounts of aryl isoprenoids and isorenieratane (near the detection limit) for the investigated sections (C_{13}–C_{22} aryl isoprenoids average 9.04, 3.37 and 10.98 μg/g TOC for the BMC, IG, and WCB sections, respectively; Haddad et al., 2016) are several orders of magnitude lower than those reported from euxinic basins (e.g., 2723 μg/g TOC for C_{14}–C_{27} aryl isoprenoid during the Changhsingian leading into the Permian–Triassic mass extinction event at the Meishan section, South China; Cao et al., 2009). This further supports that the local marine redox conditions in the Appalachian basin during the F—F interval were not persistantly euxinic (Boyer et al., 2014; Haddad et al., 2016, 2018; Kelly et al., 2019).

Ocean anoxia/euxinia has been frequently linked with the F—F mass extinction event. Albeit not recorded in our study, widespread and intermitnent ocean anoxia has been reported for F—F sections globally. In contrast, the absence of evidence for ocean anoxia, or even more oxygenated ocean, has been shown in several sections, such as Australia (Becker et al., 1991; George et al., 2014), North America (Bratton et al., 1999; White et al., 2018), and South China (Song et al., 2017) (see a review by Carmichael et al., 2019 for a summary of the redox states of global F—F sections). Heterogeneity in nutrient supply, local depositional conditions, and the living organism species is expected within a global ocean system for any interval of Earth history. Further high-resolution studies with sections that have clear biostratigraphy characterization are needed for section correlation and to determine the timing and locality of ocean anoxia, and to correlate ocean anoxia with the F—F mass extinction event.

In addition, elevated nutrient supply from enhanced terrestrial input might have boosted the marine productivity. Increased burial of marine organic matter and inert carbon (e.g., charcoal, soot) would have lead to a positive CIE and the drawdown of the pCO_2, and cause climate cooling that may have ultimately contributed to the F—F event (Averbuch et al., 2005; Huang et al., 2018; Joachimski and Buggisch, 2002; Song et al., 2017). Paleontology studies suggest that faunas living in warm temperatures were sensitive to cooling, and experienced more severe losses than faunas living in cooler water temperatures (McGhee, 1996; Ma et al., 2016). For example, over 90% of all brachiopod families from the low-latitude, tropical regions became extinct, in comparison with ~27% brachiopods from the cooler waters (McGhee, 1996). Warm-adapted benthic ostracods were also severely affected, whereas sponges and solitary rugose corals that lived in deep water environments were less affected (Ma et al., 2016). After the F—F mass extinction, faunas (e.g., foraminifers) that previously populated high-latitude regions migrated to low-latitude regions, with the low-latitude organisms that survived displaying a dramatic decline in their biogeographic distribution (Kalvoda, 1990). In addition to the mass extinction in the marine realm, research has shown that the F—F biotic crisis also affected the terrestrial ecosystems to some extent (McGhee, 1996). The ecological selectivity of the F—F biotic crisis is better explained by climate cooling. In summary, our organic geochemistry data do not provide evidence for enhanced ocean anoxia in the Appalachian basin, and whether ocean anoxia is a killing mechanism of the F—F mass extinction still needs further research. The increased frequency of wildfires fit with the climate cooling scenario across the F—F boundary interval.

6. Conclusions

The PAHs data from three F—F sections suggest enhanced wildfire activity around the FFB (Fig. 2). The dominance of three-ring Phenanthrene indicates that the wildfire has a low burning intensity. Average chain length data remained relatively constant at 29 for all three sections, and thus indicate relative aridity conditions were stable during this time interval. The enhanced wildfire activity might be linked to an elevated atmospheric oxygen level. Although a slightly increased terrestrial input was observed, no major oceanic oxygen deficiency in the Appalachian basin is detected over the F—F interval by Pr/Ph, albeit that widespread and intermittent ocean anoxia has been reported. Nevertheless, our evidence for enhanced wildfire activity corroborates with the hypothesis that pCO_2 drawdown and climate cooling that resulted from enhanced mountain building and continental weathering might have led to the F—F biocrisis. This interpretation seems more

consistent with the pattern that shallow water species were among those most severely affected.

Supplementary data to this article can be found online at https://doi.org/10.1016/j.gloplacha.2022.103904.

Declaration of Competing Interest

The authors declare no conflict of interest. This manuscript has not been submitted and will not be submitted to any other journals while it is under review for *Global and Planetary Change*.

Data availability

All the data have been included in the supplementary materials.

Acknowledgements

We acknowledge the Natural Science Foundation of China (41925014) to HT, (41790452) to JH, and the China Postdoctoral Science Foundation (20M682934) and Director's Fund of Guangzhou Institute of Geochemistry, CAS to ZL.

References

Archibald, S., Lehmann, C.E.R., Belcher, C.M., Bond, W.J., Bradstock, R.A., Daniau, A.L., Dexter, K.G., Forrestel, E.J., Greve, M., He, T., Higgins, S.I., Hoffmann, W.A., Lamont, B.B., McGlinn, D.J., Moncrieff, G.R., Osborne, C.P., Pausas, J.G., Price, O., Ripley, B.S., Rogers, B.M., Schwilk, D.W., Simon, M.F., Turetsky, M.R., Van der Werf, G.R., Zanne, A.E., 2018. Biological and geophysical feedbacks with fire in the Earth system. Environ. Res. Lett. 13, 033003.

Arinobu, T., Ishiwatari, R., Kaiho, K., Lamolda, M.A., 1999. Spike of pyrosynthetic polycyclic aromatic hydrocarbons associated with an abrupt decrease in δ13C of a terrestrial biomarker at the Cretaceous-Tertiary boundary at Caravaca, Spain. Geology 27, 723–726.

Averbuch, O., Tribovillard, N., Devleeschouwer, X., Riquier, L., Mistiaen, B., van Vliet-Lanoe, B., 2005. Mountain building-enhanced continental weathering and organic carbon burial as major causes for climatic cooling at the Frasnian-Famennian boundary (c. 376 Ma)? Terra Nova 17, 25–34.

Barkley, A.E., Prospero, J.M., Mahowald, N., Hamilton, D.S., Popendorf, K.J., Oehlert, A. M., Pourmand, A., Gatineau, A., Panechou-Pulcherie, K., Blackwelder, P., Gaston, C. J., 2019. African biomass burning is a substantial source of phosphorus deposition to the Amazon, Tropical Atlantic Ocean, and Southern Ocean. Proc. Natl. Acad. Sci. 116, 16216–16221.

Becker, R.T., House, M.R., Kirchgasser, W.T., Playford, P.E., 1991. Sedimentary and faunal changes across the frasnian/famennian boundary in the canning basin of Western Australia. Hist. Biol. 5, 183–196.

Belcher, C.M., Finch, P., Collinson, M.E., Scott, A.C., Grassineau, N.V., 2009. Geochemical evidence for combustion of hydrocarbons during the K-T impact event. Proc. Natl. Acad. Sci. 106, 4112–4117.

Belcher, C.M., Yearsley, J.M., Hadden, R.M., McElwain, J.C., Rein, G., 2010. Baseline intrinsic flammability of Earth's ecosystems estimated from paleoatmospheric oxygen over the past 350 million years. Proc. Natl. Acad. Sci. 107, 22448–22453.

Bond, D.P.G., Wignall, P.B., 2008. The role of sea-level change and marine anoxia in the Frasnian–Famennian (Late Devonian) mass extinction. Palaeogeogr. Palaeoclimatol. Palaeoecol. 263, 107–118.

Bond, D., Wignall, P.B., Racki, G., 2004. Extent and duration of marine anoxia during the Frasnian–Famennian (Late Devonian) mass extinction in Poland, Germany, Austria and France. Geol. Mag. 141, 173–193.

Boudinot, F.G., Sepúlveda, J., 2020. Marine organic carbon burial increased forest fire frequency during Oceanic Anoxic Event 2. Nat. Geosci. 13, 693–698.

Boyer, D.L., Haddad, E.E., Seeger, E.S., 2014. The last gasp: trace fossils track deoxygenation leading into the Frasnian-Famennian extinction event. Palaios 29, 646–651.

Boyer, D.L., Martinez, A.M., Evans, S.D., Cohen, P.A., Haddad, E.E., Pippenger, K.H., Love, G.D., Droser, M.L., 2021. Living on the edge: the impact of protracted oxygen stress on life in the Late Devonian. Palaeogeogr. Palaeoclimatol. Palaeoecol. 566, 110226.

Bratton, J.F., Berry, W.B.N., Morrow, J.R., 1999. Anoxia pre-dates Frasnian–Famennian boundary mass extinction horizon in the Great Basin, USA. Palaeogeogr. Palaeoclimatol. Palaeoecol. 154, 275–292.

Bush, R.T., McInerney, F.A., 2013. Leaf wax n-alkane distributions in and across modern plants: implications for paleoecology and chemotaxonomy. Geochim. Cosmochim. Acta 117, 161–179.

Cao, C., Love, G.D., Hays, L.E., Wang, W., Shen, S., Summons, R.E., 2009. Biogeochemical evidence for euxinic oceans and ecological disturbance presaging the end-Permian mass extinction event. Earth Planet. Sci. Lett. 281, 188–201.

Carmichael, S.K., Waters, J.A., Suttner, T.J., Kido, E., DeReuil, A.A., 2014. A new model for the Kellwasser Anoxia Events (Late Devonian): Shallow water anoxia in an open oceanic setting in the Central Asian Orogenic Belt. Palaeogeogr. Palaeoclimatol. Palaeoecol. 399, 394–403.

Carmichael, S.K., Waters, J.A., Königshof, P., Suttner, T.J., Kido, E., 2019. Paleogeography and paleoenvironments of the Late Devonian Kellwasser event: a review of its sedimentological and geochemical expression. Glob. Planet. Chang. 183, 102984.

Carr, A.S., Boom, A., Grimes, H.L., Chase, B.M., Meadows, M.E., Harris, A., 2014. Leaf wax n-alkane distributions in arid zone South African flora: environmental controls, chemotaxonomy and palaeoecological implications. Org. Geochem. 67, 72–84.

Claeys, P., Casier, J.-G., Margolis, S.V., 1992. Microtektites and Mass Extinctions: evidence for a Late Devonian Asteroid Impact. Science 257, 1102–1104.

Cohen, P.A., Junium, C.K., King Phillips, E., Uveges, B.T., 2021. Carbon cycle dynamics and ecology revealed by the carbon isotopic composition of single organic microfossils during the Late Devonian Biotic Crisis. Geobiology n/a. 20 (3), 346–362.

Copper, P., 2002. Reef development at the Frasnian/Famennian mass extinction boundary. Palaeogeogr. Palaeoclimatol. Palaeoecol. 181, 27–65.

Dahl, T.W., Hammarlund, E.U., Anbar, A.D., Bond, D.P.G., Gill, B.C., Gordon, G.W., Knoll, A.H., Nielsen, A.T., Schovsbo, N.H., Canfield, D.E., 2010. Devonian rise in atmospheric oxygen correlated to the radiations of terrestrial plants and large predatory fish. Proc. Natl. Acad. Sci. 107, 17911–17915.

Diefendorf, A.F., Freeman, K.H., Wing, S.L., Graham, H.V., 2011. Production of n-alkyl lipids in living plants and implications for the geologic past. Geochim. Cosmochim. Acta 75, 7472–7485.

Eglinton, G., Hamilton, R.J., 1967. Leaf epicuticular waxes. Science 156, 1322–1335.

Finkelstein, D.B., Pratt, L.M., Curtin, T.M., Brassel, S.C., 2005. Wildfires and seasonal aridity recorded in late cretaceous strata from south-eastern Arizona, USA. Sedimentology 52, 587–599.

George, A.D., Chow, N., Trinajstic, K.M., 2014. Oxic facies and the Late Devonian mass extinction, Canning Basin, Australia. Geology 42, 327–330.

Glasspool, I.J., Scott, A.C., 2010. Phanerozoic concentrations of atmospheric oxygen reconstructed from sedimentary charcoal. Nat. Geosci. 3, 627.

Glasspool, I.J., Scott, A.C., Waltham, D., Pronina, N., Shao, L., 2015. The impact of fire on the Late Paleozoic Earth system. Front. Plant Sci. 6.

Gordon, G.W., Rockman, M., Turekian, K.K., Over, J., 2009. Osmium isotopic evidence against an impact at the Frasnian-Famennian boundary, 309, pp. 420–430.

Haddad, E.E., Tuite, M.L., Martinez, A.M., Williford, K., Boyer, D.L., Droser, M.L., Love, G.D., 2016. Lipid biomarker stratigraphic records through the Late Devonian Frasnian/Famennian boundary: comparison of high- and low-latitude epicontinental marine settings. Org. Geochem. 98, 38–53.

Haddad, E.E., Boyer, D.L., Droser, M.L., Lee, B.K., Lyons, T.W., Love, G.D., 2018. Ichnofabrics and chemostratigraphy argue against persistent anoxia during the Upper Kellwasser Event in New York State. Palaeogeogr. Palaeoclimatol. Palaeoecol. 490, 178–190.

Harris, N.B., Mnich, C.A., Selby, D., Korn, D., 2013. Minor and trace element and Re–Os chemistry of the Upper Devonian Woodford Shale, Permian Basin, West Texas: insights into metal abundance and basin processes. Chem. Geol. 356, 76–93.

Heimhofer, U., Wucherpfennig, N., Adatte, T., Schouten, S., Schneebeli-Hermann, E., Gardin, S., Keller, G., Kentsch, S., Kujau, A., 2018. Vegetation response to exceptional global warmth during Oceanic Anoxic Event 2. Nat. Commun. 9, 3832.

Hoffmann, B., Kahmen, A., Cernusak, L.A., Arndt, S.K., Sachse, D., 2013. Abundance and distribution of leaf wax n-alkanes in leaves of Acacia and Eucalyptus trees along a strong humidity gradient in northern Australia. Org. Geochem. 62, 62–67.

Huang, C., Joachimski, M.M., Gong, Y., 2018. Did climate changes trigger the Late Devonian Kellwasser Crisis? Evidence from a high-resolution conodont $\delta^{18}O_{PO4}$ record from South China. Earth Planet. Sci. Lett. 495, 174–184.

Jaffe, L.A., Peucker-Ehrenbrink, B., Petsch, S.T., 2002. Mobility of rhenium, platinum group elements and organic carbon during black shale weathering. Earth Planet. Sci. Lett. 198, 339–353.

Jiang, C., Alexander, R., Kagi, R.I., Murray, A.P., 1998. Polycyclic aromatic hydrocarbons in ancient sediments and their relationships to palaeoclimate. Org. Geochem. 29, 1721–1735.

Joachimski, M.M., Buggisch, W., 2002. Conodont apatite $\delta^{18}O$ signatures indicate climatic cooling as a trigger of the Late Devonian mass extinction. Geology 30, 711–714.

Joachimski, M.M., Breisig, S., Buggisch, W., Talent, J.A., Mawson, R., Gereke, M., Morrow, J.R., Day, J., Weddige, K., 2009. Devonian climate and reef evolution: insights from oxygen isotopes in apatite. Earth Planet. Sci. Lett. 284, 599–609.

Johnson, J.G., Klapper, G., Sandberg, C.A., 1985. Devonian Eustatic fluctuations in Euramerica. Geol. Soc. Am. Bull. 96, 567–587.

Kaiho, K., Yatsu, S., Oba, M., Gorjan, P., Casier, J.-G., Ikeda, M., 2013. A forest fire and soil erosion event during the Late Devonian mass extinction. Palaeogeogr. Palaeoclimatol. Palaeoecol. 392, 272–280.

Kaiho, K., Miura, M., Tezuka, M., Hayashi, N., Jones, D.S., Oikawa, K., Casier, J.-G., Fujibayashi, M., Chen, Z.-Q., 2021. Coronene, mercury, and biomarker data support a link between extinction magnitude and volcanic intensity in the Late Devonian. Glob. Planet. Chang. 199, 103452.

Kalvoda, J., 1990. Late Devonian — Early Carboniferous paleobiogeography of benthic Foraminifera and climatic oscillations. In: Kauffman, E.G., Walliser, O.H. (Eds.), Extinction Events in Earth History. Springer Berlin Heidelberg, Berlin, Heidelberg, pp. 183–187.

Kaufmann, B., Trapp, E., Mezger, K., 2004. The numerical age of the upper Frasnian (Upper Devonian) Kellwasser horizons: a new U-Pb zircon date from Steinbruch Schmidt (Kellerwald, Germany). J. Geol. 112, 495–501.

Kelly, A.A., Cohen, P.A., Boyer, D.L., 2019. Tiny keys to unlocking the Kellwasser events: detailed characterization of organic walled microfossils associated with extinction in western New York State. Palaios 34, 96–104.
Killops, S.D., Massoud, M.S., 1992. Polycyclic aromatic hydrocarbons of pyrolytic origin in ancient sediments: evidence for Jurassic vegetation fires. Org. Geochem. 18, 1–7.
Klapper, G., Feist, R., Becker, R.T., House, M.R., 1993. Definition of the Frasnian Famennian Stage Boundary. Episodes 16, 433–441.
Koopmans, M.P., Rijpstra, W.I.C., Klapwijk, M.M., de Leeuw, J.W., Lewan, M.D., Sinninghe Damsté, J.S., 1999. A thermal and chemical degradation approach to decipher pristane and phytane precursors in sedimentary organic matter. Org. Geochem. 30, 1089–1104.
Krause, A.J., Mills, B.J.W., Zhang, S., Planavsky, N.J., Lenton, T.M., Poulton, S.W., 2018. Stepwise oxygenation of the Paleozoic atmosphere. Nat. Commun. 9, 4081.
Lash, G.G., 2017. A multiproxy analysis of the Frasnian-Famennian transition in western New York State, U.S.A. Palaeogeogr. Palaeoclimatol. Palaeoecol. 473, 108–122.
Lenton, T.M., Daines, S.J., Mills, B.J.W., 2018. COPSE reloaded: an improved model of biogeochemical cycling over Phanerozoic time. Earth Sci. Rev. 178, 1–28.
Lima, A.L.C., Farrington, J.W., Reddy, C.M., 2005. Combustion-derived polycyclic aromatic hydrocarbons in the environment—a review. Environ. Forensic 6, 109–131.
Liu, Z., Selby, D., Hackley, P.C., Over, D.J., 2020. Evidence of wildfires and elevated atmospheric oxygen at the Frasnian–Famennian boundary in New York (USA): Implications for the Late Devonian mass extinction. GSA Bull. 132 (9–10), 2043–2054.
Liu, Z., Percival, L.M.E., Vandeputte, D., Selby, D., Claeys, P., Over, D.J., Gao, Y., 2021. Upper Devonian mercury record from North America and its implications for the Frasnian–Famennian mass extinction. Palaeogeogr. Palaeoclimatol. Palaeoecol. 576, 110502.
Lu, M., Lu, Y., Ikejiri, T., Sun, D., Carroll, R., Blair, E.H., Algeo, T.J., Sun, Y., 2021. Periodic oceanic euxinia and terrestrial fluxes linked to astronomical forcing during the Late Devonian Frasnian–Famennian mass extinction. Earth Planet. Sci. Lett. 562, 116839.
Ma, X., Gong, Y., Chen, D., Racki, G., Chen, X., Liao, W., 2016. The Late Devonian Frasnian–Famennian Event in South China — patterns and causes of extinctions, sea level changes, and isotope variations. Palaeogeogr. Palaeoclimatol. Palaeoecol. 448, 224–244.
Marynowski, L., Filipiak, P., 2007. Water column euxinia and wildfire evidence during deposition of the Upper Famennian Hangenberg event horizon from the Holy Cross Mountains (central Poland). Geol. Mag. 144, 569–595.
Marynowski, L., Simoneit, B.R.T., 2009. Widespread Upper Triassic to Lower Jurassic wildfire records from Poland: evidence from charcoal and pyrolytic polycyclic aromatic hydrocarbons. Palaios 24, 785–798.
Marynowski, L., Kurkiewicz, S., Rakociński, M., Simoneit, B.R.T., 2011. Effects of weathering on organic matter: I. Changes in molecular composition of extractable organic compounds caused by paleoweathering of a Lower Carboniferous (Tournaisian) marine black shale. Chem. Geol. 285, 144–156.
Masclet, P., Pistikopoulos, P., Beyne, S., Mouvier, G., 1988. Long range transport and gas/particle distribution of polycyclic aromatic hydrocarbons at a remote site in the Mediterranean Sea. Atmos. Environ. 1967 (22), 639–650.
Masclet, P., Cachier, H., Liousse, C., Wortham, H., 1995. Emissions of polycyclic aromatic hydrocarbons by savanna fires. J. Atmos. Chem. 22, 41–54.
McGhee, G.R., 1996. The Late Devonian Mass Extinction: The Frasnian/Famennian Crisis. Columbia University Press.
Over, D.J., 1997. Conodont biostratigraphy of the Java Formation (Upper Devonian) and the Frasnian-Famennian boundary in western New York State. In: Klapper, G., Murphy, M.A., Talent, J.A. (Eds.), Paleozoic Sequence Stratigraphy, Biostratigraphy, and Biogeography: Studies in Honor of J. Granville ("Jess") Johnson. Geological Society of America, pp. 161–177.
Over, D.J., 2002. The Frasnian/Famennian boundary in central and eastern United States. Palaeogeogr. Palaeoclimatol. Palaeoecol. 181, 153–169.
Percival, L.M.E., Davies, J.H.F.L., Schaltegger, U., De Vleeschouwer, D., Da Silva, A.C., Föllmi, K.B., 2018. Precisely dating the Frasnian–Famennian boundary: implications for the cause of the Late Devonian mass extinction. Sci. Rep. 8, 9578.
Peters, K.E., Peters, K.E., Walters, C.C., Moldowan, J., 2005. The Biomarker Guide. Cambridge University Press.
Racki, G., Rakociński, M., Marynowski, L., Wignall, P.B., 2018. Mercury enrichments and the Frasnian-Famennian biotic crisis: a volcanic trigger proved? Geology 46, 543–546.
Rimmer, S.M., Hawkins, S.J., Scott, A.C., Cressler, W.L., 2015. The rise of fire: fossil charcoal in late Devonian marine shales as an indicator of expanding terrestrial ecosystems, fire, and atmospheric change. Am. J. Sci. 315, 713–733.
Sageman, B.B., Murphy, A.E., Werne, J.P., Ver Straeten, C.A., Hollander, D.J., Lyons, T. W., 2003. A tale of shales: the relative roles of production, decomposition, and dilution in the accumulation of organic-rich strata, Middle–Upper Devonian, Appalachian basin. Chem. Geol. 195, 229–273.
Schachat, S.R., Labandeira, C.C., Saltzman, M.R., Cramer, B.D., Payne, J.L., Boyce, C.K., 2018. Phanerozoic pO_2 and the early evolution of terrestrial animals. Proc. R. Soc. B 285, 20172631.
Schmidt, M.W.I., Noack, A.G., 2000. Black carbon in soils and sediments: analysis, distribution, implications, and current challenges. Glob. Biogeochem. Cycles 14, 777–793.
Scott, A.C., Glasspool, I.J., 2006. The diversification of Paleozoic fire systems and fluctuations in atmospheric oxygen concentration. Proc. Natl. Acad. Sci. 103, 10861–10865.
Shen, W., Sun, Y., Lin, Y., Liu, D., Chai, P., 2011. Evidence for wildfire in the Meishan section and implications for Permian–Triassic events. Geochim. Cosmochim. Acta 75, 1992–2006.
Shen, J., Feng, Q., Algeo, T.J., Liu, J., Zhou, C., Wei, W., Liu, J., Them, T.R., Gill, B.C., Chen, J., 2020. Sedimentary host phases of mercury (Hg) and implications for use of Hg as a volcanic proxy. Earth Planet. Sci. Lett. 543, 116333.
Song, H., Song, H., Algeo, T.J., Tong, J., Romaniello, S.J., Zhu, Y., Chu, D., Gong, Y., Anbar, A.D., 2017. Uranium and carbon isotopes document global-ocean redox-productivity relationships linked to cooling during the Frasnian-Famennian mass extinction. Geology 45, 887–890.
Song, Y., Gilleaudeau, G.J., Algeo, T.J., Over, D.J., Lyons, T.W., Anbar, A.D., Xie, S., 2020. Biomarker evidence of algal-microbial community changes linked to redox and salinity variation, Upper Devonian Chattanooga Shale (Tennessee, USA). GSA Bull. https://doi.org/10.1130/B35543.1.
Spalletta, C., Perri, M.C., Over, D.J., Corradini, C., 2017. Famennian (Upper Devonian) conodont zonation: revised global standard. Bull. Geosci. 92, 31–57.
Stanley, S.M., 2016. Estimates of the magnitudes of major marine mass extinctions in earth history. Proc. Natl. Acad. Sci. U. S. A. 113, E6325–E6334.
Stein, W.E., Berry, C.M., Hernick, L.V., Mannolini, F., 2012. Surprisingly complex community discovered in the mid-Devonian fossil forest at Gilboa. Nature 483, 78.
Summons, R.E., Powell, T.G., 1986. Chlorobiaceae in Palaeozoic seas revealed by biological markers, isotopes and geology. Nature 319, 763–765.
Turgeon, S.C., Creaser, R.A., Algeo, T.J., 2007. Re–Os depositional ages and seawater Os estimates for the Frasnian–Famennian boundary: implications for weathering rates, land plant evolution, and extinction mechanisms. Earth Planet. Sci. Lett. 261, 649–661.
Uveges, B.T., Junium, C.K., Boyer, D.L., Cohen, P.A., Day, J.E., 2019. Biogeochemical controls on black shale deposition during the Frasnian-Famennian biotic crisis in the Illinois and Appalachian Basins, USA, inferred from stable isotopes of nitrogen and carbon. Palaeogeogr. Palaeoclimatol. Palaeoecol. 531, 108787.
Venkatesan, M.I., Dahl, J., 1989. Organic geochemical evidence for global fires at the Cretaceous/Tertiary boundary. Nature 338, 57–60.
Vogts, A., Schefuß, E., Badewien, T., Rullkötter, J., 2012. n-Alkane parameters from a deep sea sediment transect off southwest Africa reflect continental vegetation and climate conditions. Org. Geochem. 47, 109–119.
Watson, A.J., Lovelock, J.E., 2013. The Dependence of Flame Spread and Probability of Ignition on Atmospheric Oxygen, Fire Phenomena and the Earth System, pp. 273–287.
White, D.A., Elrick, M., Romaniello, S., Zhang, F., 2018. Global seawater redox trends during the Late Devonian mass extinction detected using U isotopes of marine limestones. Earth Planet. Sci. Lett. 503, 68–77.
Zhao, H., Shen, J., Algeo, T.J., Racki, G., Chen, J., Huang, C., Song, J., Qie, W., Gong, Y., 2022. Mercury isotope evidence for regional volcanism during the Frasnian-Famennian transition. Earth Planet. Sci. Lett. 581, 117412.